Received July 9, 2019, accepted July 26, 2019, date of publication August 2, 2019, date of current version August 26, 2019.

Digital Object Identifier 10.1109/ACCESS.2019.2932956

Dynamic Control of Virtual Hand Grasp Using Spatiotemporal Synergies

MARTIN K. BURNS, (Student Member, IEEE), DINGYI PEI, (Student Member, IEEE), AND RAMANA VINJAMURI, (Senior Member, IEEE)
Stevens Institute of Technology, Hoboken, NJ 07030, USA

Corresponding author: Ramana Vinjamuri (ramana.vinjamuri@stevens.edu)

This work was supported by the New Jersey Health Foundation (NJHF) under Grant PC76-16 and by the National Science Foundation (NSF) under Grant CHS-1845197.

ABSTRACT Recent advances in assistive hand devices have produced high degree of freedom systems which are capable of complex grasping, however user-friendly control of these sophisticated devices is still an open topic in research. Synergy-based controllers which dimensionally reduced the control problem were present in the literature, however they used spatial/postural synergies which are static over time. In this paper, we proposed the first control system based on spatiotemporal synergies which is scalable to any number of degrees of freedom, any number of synergies, and any duration of synergy. The controller was tested on prior data in which ten subjects performed 50 object grasps and 36 American Sign Language letters and numbers. The tuned response of the controller, the l_1-norm reconstruction error, and the simulation error were all reported in detail. The angular error between the simulated model and recorded states decayed rapidly from 23.1±19.98% with the first synergy to 6.18±8.75% for synergies 1 to 6 and 2.29±3.35% for synergies 1 to 10 and was statistically similar to the reconstruction error of the angular trajectories. Minor improvements in performance were observed when using higher-order synergies, implying a tradeoff between accuracy and control complexity. The data shown here can be used to select the number of synergies to use in control based on the accuracy of the controller and the accuracy of the controlled robotic system. The resulting system achieved high grasping dexterity with minimal computational or manual effort for assistive devices.

INDEX TERMS Assistive devices, prosthetics, dimensionality reduction, exoskeleton, kinematics, object grasping, robotics and controls, spatiotemporal synergies, torque control, virtual hand.

I. INTRODUCTION

Individuals who experience paralysis or loss of a limb risk losing their ability to independently conduct activities of daily living (ADL). Out of the 185,000 individuals who suffer limb loss every year in the US [1], 15% will undergo a transradial and 8% will undergo a transhumeral amputation [2]. Stroke alone, affecting an estimated 795,000 individuals per year [3], leaves 65% unable to integrate their affected hand into normal activities six months post-stroke [4]. Some hand function can be restored through diligent rehabilitation, however those who do not regain enough function for ADL face hardships. The persistent loss of hand function for ADL reduces the individual's ability to independently care for themselves and drastically affects their quality of life. This manifests as financial, emotional, social, and mental hardship on the affected individual and their loved ones or close caretakers [5]. Assistive devices such as prosthetics and wearable robotics offer a promising method of reducing this functional gap, however more development needs to be undergone before they become ubiquitous.

The control and function of assistive devices are among the most commonly-cited needs for improvement in prosthetics and wearable robotics for the upper limb [6]. Hand prosthetics and exoskeletons aim to improve device dexterity beyond single degree of freedom (DoF) hand open-close motions by increasing the number of independently actuated joints. This leads to more sophisticated devices capable of a richer variety of hand motions, however the added DoF leads to increased difficulty for the user to control. A user may be able to control several DoF using as many muscles through electromyography (EMG), however it is not possible to fully control,

The associate editor coordinating the review of this manuscript and approving it for publication was Cihun-Siyong Gong.

for instance, the 26-DoF Modular Prosthetic Limb with this method. There has been a significant push to maintain the dexterousness of high-DoF devices without increasing the control complexity for the user.

One approach to simplify the control of high-DoF devices is based on basic science research in motor neurophysiology. High-DoF biological systems, such as the limbs of animals and hands of humans, were hypothesized to be controlled by relatively few patterns of motion during normal operation [7]. This hypothesis was supported by experiments in frogs [8] and cats [9] which showed coupled activations of muscles of the limb when stimulating individual neurons in the spinal cord. Furthermore, the motion patterns observed as a result of neural stimulations showed significant correlation with the motor patterns derived from kinematic observations [10]. This coordinated behavior was also observed during cortical stimulation, demonstrating that the surface areas dedicated to activating particular muscles or motor units overlapped in the motor cortex [11]. This experimental evidence was formulated into the concept of synergies, or ''a collection of relatively independent degrees of freedom that behave as a single functional unit'' [12]. These functional units or movement patterns serve as building blocks of movement which can be summed and scaled to reproduce hand and arm motion. Kinematic synergies are movement patterns defined in terms of kinematic states of the system (joint angles/angular velocities) while muscular synergies are defined in terms of co-activations of muscles. These categories can be further divided into postural/spatial synergies, in which the activation patterns are constant in time, and spatiotemporal synergies, in which these patterns of activation change over a certain time duration. These synergies can be biomechanically derived using decomposition tools to extract linearly independent motion profiles from reach and grasp data [13] and have been used in several applications including brain-computer interfaces (BCIs) [14], hand grasp reconstruction [15], and bilateral arm reaching reconstruction [16].

Synergies have been demonstrated experimentally and computationally, so research groups have integrated these motion patterns into systems aimed at replicating and assisting grasps used in ADL. Synergies are mathematically represented as a set of linearly independent vectors, with coordinates in these vectors being referred to as synergy recruitments or weights. Some notable groups have realized these vectors as mechanisms which convert motion of relatively few actuators into whole-hand motion of the joints of a prosthetic or exoskeleton hand [17]–[21]. Other groups have designed control laws which operate on the mathematical definition of synergies. Notably, the DLR hand was controlled using an impedance control law operating in the synergy recruitment domain to implement two synergies, with a method that is scalable to any number of synergies desired [22]. Postural kinematic and muscle synergies were used to successfully estimate hand endpoint trajectories from EMG signals of the upper limb [23]. Several groups have used hand synergies to perform autonomous grasp planning [24]–[26] and object manipulation [27].

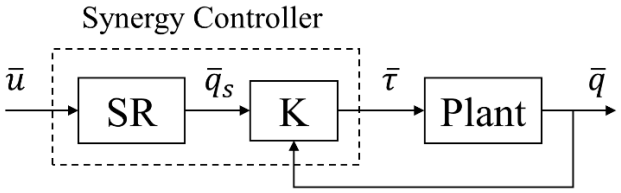

FIGURE 1. General block diagram of the synergy controller. A synergy recruiter (SR) converts the synergy recruitments weights, $\bar{u}$, into joint setpoints $\bar{q}_s$. A control law (K) compares the plant states, $\bar{q}$, and the setpoints and computes a compensatory torque $\bar{\tau}$.

With the exception of [19], the vast majority of synergy implementations in prosthetic and exoskeleton hands have used postural, or time-invariant synergies. These synergies encode linear relationships between the joints of the hand while representing a significant amount of variability in measured grasp data. However, these synergies are derived from grasp end postures, and so do not encode the complex dynamics of the hand during reaching and grasping. Spatiotemporal synergies are extracted from the entire object grasping timeseries, and so encode the subtle variations in motion during the grasp process. The major drawback is that their time-varying nature is difficult to integrate into control laws, which typically operate on a sample-to-sample basis without considering a forward trajectory.

In this paper, we present the first control system based on spatiotemporal synergies. A state space synergy recruitment system is designed which converts synergy recruitment weights into angle and angular velocity trajectories for the hand. A control law based on the state space representation is used to control a virtual hand implemented in Simulink. This simulated system is used to replicate natural-paced grasping and American Sign Language data previously captured and shown in [13]. We hypothesize that the synergy controller can actuate the virtual hand along a synergy trajectory, and that it can sufficiently replicate reach-to-grasp movements representative of ADL grasping given enough synergies.

II. MATERIAL AND METHODS

In general, we wish to implement a control system of the form shown in Fig. 1. The system accepts a time-series of m synergy recruitments, $\bar{u} \in \mathbb{R}^m$, and actuates a plant which can be a virtual, prosthetic, or wearable robotic system along J DoF, of which the full state $\bar{q} \in \mathbb{R}^{2*J}$ includes angles and velocities for each DoF. For high-DoF systems we want to simplify the control problem by setting $m < J$. The synergy controller is composed of two subsystems: a Synergy Recruiter (SR) and a control law (K). The SR expands the low-dimensional control inputs in the synergy domain into high-dimensional commands in the plant's state space. The control law uses these commands and observations of the plant's current state to apply a control input to the plant. Our SR, therefore, needs

to map $\bar{u} \Rightarrow \bar{q}_s \in \mathbb{R}^{2*J}$ according to trajectories defined by spatiotemporal synergies, where $\bar{q}_s$ is a vector of full-state setpoints of the J-DoF plant. We accomplish this with a discrete state space system.

A. STATE SPACE SYNERGY RECRUITMENT MODEL

A discrete state space model for our inputs $\bar{u}$ and outputs $\bar{q}_s$ is written as

$$\bar{x}_+ = A\bar{x}_- + B\bar{u} \tag{1}$$

$$\bar{q}_s = C\bar{x}_+ + D\bar{u} \tag{2}$$

where $\bar{x}$ is an internal state and A, B, C, and D are matrices. For our system, we always assume $D = [0]$. $\bar{x}_-$ and $\bar{x}_+$ are the prior and propagated state. Our input, or recruitment weights, and output vectors, or state setpoints, are defined as

$$\bar{u} = \begin{bmatrix} u_1 & u_2 & \dots & u_m \end{bmatrix}^T \tag{3}$$

$$\bar{q}_s = \begin{bmatrix} \theta_1 & \theta_2 & \dots & \theta_J & \omega_1 & \omega_2 & \dots & \omega_J \end{bmatrix}^T \tag{4}$$

where u_m is the synergy recruitment for the m^{th} synergy and θ_j and ω_j are the angles and angular velocities for the j^{th} DoF of the system. We choose our $\bar{x}$ vector to be the angles and angular velocities of the current timestep for the system as well as the angular velocities for the next T timepoints, where T is the duration of our spatiotemporal synergies in samples.

$$\bar{x} = \begin{bmatrix} \bar{\theta}(1) & \bar{\omega}(1) & \bar{\omega}(2) & \dots & \bar{\omega}(T) \end{bmatrix}^{\mathrm{T}} \tag{5}$$

With this format, we design the A matrix to numerically integrate the instantaneous velocity into the current angles and to advance the future velocities one timestep:

$$A = \begin{bmatrix} I^{J\times J} & \Delta t * I^{J\times J} & 0^{J\times(J*T-J)} \\ 0^{(J*T-J)\times 2J} & & I^{(J*\mathrm{T-J})\times(J*T-J)} \\ & 0^{J\times(J+J*T)} & \end{bmatrix} \tag{6}$$

where $0^{R\times C} I^{R\times C}$ are zero and identity matrices of size R rows and C columns. The time step size for each sample is Δt, which is determined by the sample rate of the original synergies. Next, we encode our spatiotemporal synergies, S_m, into the B matrix:

$$S_m = \begin{bmatrix} s_1^m(1) & s_2^m(1) & \dots & s_J^m(1) \\ s_1^m(2) & s_2^m(2) & \dots & s_J^m(2) \\ & & \vdots & \\ s_1^m(T) & s_2^m(T) & \dots & s_J^m(T) \end{bmatrix} \tag{7}$$

$$B_s = \begin{bmatrix} s_1^1(1) & s_1^2(1) & & s_1^m(1) \\ s_2^1(1) & s_2^2(1) & & s_2^m(1) \\ \vdots & \vdots & \dots & \vdots \\ s_J^1(1) & s_J^2(1) & & s_J^m(1) \\ \vdots & \vdots & & \vdots \\ s_J^1(T) & s_J^2(T) & & s_J^m(T) \end{bmatrix} \tag{8}$$

$$B = \begin{bmatrix} 0^{J\times m} \\ B_s \end{bmatrix} \tag{9}$$

TABLE 1. Masses and dimensions of virtual hand model.

Body Name	Mass (g)	Inter-Joint Distance (mm)
Palm	302.02	
TP	45.89	58.11
TD	10.92	30.92
IP	16.20	39.85
IM	9.01	29.00
ID	5.22	23.73
MP	15.88	37.39
MM	10.22	32.30
MD	6.02	27.82
RP	12.93	33.85
RM	8.58	31.02
RD	5.25	24.76
PP	10.63	32.37
PM	3.80	19.60
PD	3.24	21.87
Total:	465.79	

Each of the m matrices S_m have J joints defined across columns and T time samples defined across rows. These are reformatted into a new synergy matrix, B_s, which encodes each of the m synergies along columns and the $J * T$ joints at each instant of time across the rows. The C matrix is now defined as

$$C = I^{2*J\times(J*T+J)} \tag{10}$$

which returns only the current angles and angular velocities to $\bar{q}_s$. We can verify the observability of the system independent of the specific synergy profiles by computing the rank of the observability matrix O:

$$rank\left(\begin{bmatrix} C & CA & \dots & CA^{n-1} \end{bmatrix}^T\right) = JT + J \tag{11}$$

This model allows us to compute the current angle and angular velocity according to arbitrary synergies of any duration in time. For $T = 1$ this system reduces to the spatial synergy case, augmented with numerical integration to get joint angles.

B. DYNAMICS MODEL AND CONTROL LAW

The virtual hand used as the plant was created using the CADHumans model sized for a 50th percentile human male. Inertial properties including mass and center of mass were generated by applying a uniform tissue density of $1.11 g/cm^3$ [28]. The MCP and PIP joints can rotate freely between 90 degrees extension and 180 degrees flexion to accommodate the range of motion of the recorded data. The DIP joint angle is constrained to be proportional to the PIP angle with a gain of 5/7. Table I shows key parameters for the hand model, which has an overall wrist-to-fingertip length of 19.94 cm. Each body is named with the first initial of the finger followed by the first initial of the phalange, i.e. RM is

the ring finger middle phalange link. The standard form for this dynamic system is

$$M(q)\ddot{q} + C(\dot{q}, q)\dot{q} + G(q) = \tau_{int} + \tau_{ext} \quad (12)$$

which can be derived through Lagrangian mechanics. $q, \dot{q}, \ddot{q} \in \mathbb{R}^J$ are the joint angle, velocity, and acceleration vectors of the virtual hand. $M(q)$ is the postural inertia matrix,$C(\dot{q}, q)$ is the Coriolis matrix, and $G(q)$ is the vector of gravity torques. τ_{int} is the vector of internal torques of the hand model, and τ_{ext} is the external torque applied to the model. The external torque can be decomposed into two separate torques:

$$\tau_{ext} = \tau_{env} + \tau_c \quad (13)$$

where τ_{env} is the joint torques generated from interactions with the environment and τ_c is the torque applied by our controller. For this paper we assume $\tau_{int} = \tau_{env} = 0$ to simulate a healthy subject's hand operating in an open, unobstructed environment.

We compute τ_c to be a function of the desired setpoint motion, $q_s, \dot{q}_s, \ddot{q}_s$, and the measured plant kinematics

$$\tau_c = M(q)\left(\ddot{q}_s - K_d\dot{q}_e - K_p q_e\right) + C(\dot{q}, q)\dot{q} + G(q) \quad (14)$$

$$q_e = q - q_s, \dot{q}_e = \dot{q} - \dot{q}_s \quad (15)$$

where K_p and K_d are $J \times J$ tuning matrices for the angle error, q_e, and the velocity error, $\dot{q}_e$, respectively. The tuning matrices are formatted as block-diagonal matrices including the 2 controlled DoF for each finger. Each 2×2 block was tuned in isolation to achieve a step response with $10 * \Delta$t time constant, or 0.116s. The multi-input, multi-output (MIMO) control system was tuned using a model linearization about the 0-degree resting posture for all joints.

After tuning, the state space synergy recruiter was substituted into the control law by defining observer matrices for the different components of the hidden state $\bar{x}_+$:

$$q_s = C_q\bar{x}_+, \quad \dot{q}_s = C_{\dot{q}}\bar{x}_+, \ \ddot{q}_s = C_{\ddot{q}}\bar{x}_+ \quad (16)$$

$$C_q = \begin{bmatrix} I^{J\times J} & 0^{J\times J*T} \end{bmatrix} \quad (17)$$

$$C_{\dot{q}} = \begin{bmatrix} 0^{J\times J} & I^{J\times J} & 0^{J\times J*(T-1)} \end{bmatrix} \quad (18)$$

$$C_{\ddot{q}} = \Delta t * \begin{bmatrix} 0^{J\times J} & -I^{J\times J} & I^{J\times J} & 0^{J\times J*(T-2)} \end{bmatrix} \quad (19)$$

Therefore $C_q, C_{\dot{q}}, C_{\ddot{q}} \in \mathbb{R}^{J\times J*(T+1)}$. The control law in (14) receives setpoints for each DoF of the hand. Substituting (1)-(2) and (15)-(19) into (14), expanding, and regrouping terms yields a new control law which takes m spatiotemporal synergy recruitments, $\bar{u}$, as an input:

$$\tau_c = M(q)\left(C_{KA}\bar{x}_- + C_{KB}\bar{u} - K_d\dot{q} - K_p q\right) + C(\dot{q}, q)\dot{q} + G(q) \quad (20)$$

The resulting control law has one term, $C_{KA}\bar{x}_-$, which tracks the future synergy trajectory, one term, $C_{KB}\bar{u}$, receives the instantaneous synergy recruitment input, and one term each for the current plant angle and angular velocity. The difference between the synergy-generated trajectory and the virtual hand states is used to produce a desired acceleration, which is applied using torques computed from the dynamics of the hand model. The control matrices for the trajectory and input, C_{KA} and C_{KB} respectively, are constants which are initialized from the synergy model and tuning matrices:

$$C_{KA} = \left(C_{\ddot{q}} + K_d C_{\dot{q}} + K_p C_q\right) A \quad (21)$$

$$C_{KB} = \left(C_{\ddot{q}} + K_d C_{\dot{q}} + K_p C_q\right) B \quad (22)$$

We use (1) to propagate the prior state forward and (2) to observe the angle and angular velocity setpoints. The prior state is initialized as $\bar{x}_0$ to set the initial hand posture. We will use this control law to drive the virtual hand along an arbitrary trajectory based on spatiotemporal synergies, defined entirely by the timeseries of synergy gains $\bar{u}$ and the initial synergy trajectory state $\bar{x}_0$.

C. REPLICATING NATURAL GRASP/ASL POSTURES

In order to test our control system we turn to prior data in natural grasping and American Sign Language (ASL) [13], [15]. Fig. 2 shows a high-level diagram of how this data was processed to test the synergy controller. In this dataset, 10 healthy subjects performed 50 rapid-paced grasps of 25 objects consisting of spheres, discs, rectangles, pentagons, and nuts and

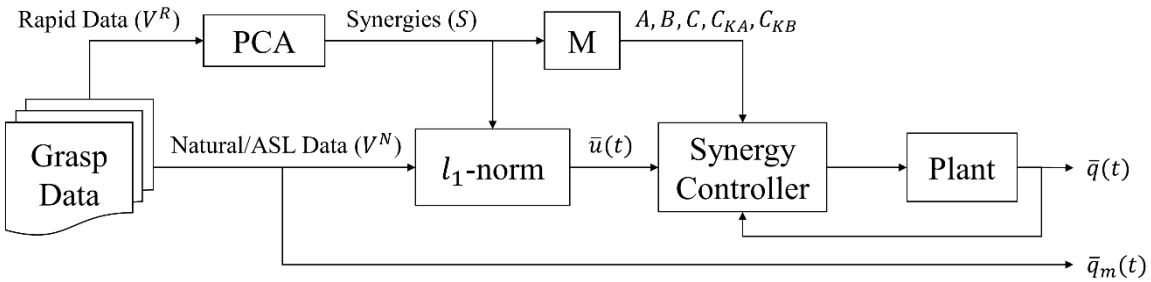

FIGURE 2. Block diagram outlining the testing scheme for the synergy controller. Rapid tasks (V_R) from the grasp data are used to derive synergies (S) using principal component analysis (PCA). The natural and ASL tasks from the grasp dataset are reconstructed using S in the l_1-norm algorithm to get $\bar{u}(t)$. The synergy control matrices are formed in M, and the resulting controller and plant are simulated using the synergy weights to produce $\bar{q}(t)$. The simulated hand states are compared to the measured states from the grasp data, $\bar{q}_m$.

bolts of various sizes. Subjects then performed 50 natural-paced grasps of the same 25 objects, then formed 36 ASL hand postures which include 26 alphabetical letters and 10 numbers. Principal Component Analysis (PCA) was used to extract spatiotemporal synergies (S) from the R rapid tasks (V^R) under the assumption that the rapid pace minimized sensory feedback and thus the data approximated an impulse response of the hand-shaping system:

$$V^R = \begin{bmatrix} v_1^1(1) & v_1^2(1) & & v_1^R(1) \\ v_2^1(1) & v_2^2(1) & & v_2^R(1) \\ \vdots & & & \vdots \\ v_J^1(1) & v_J^2(1) & \dots & v_J^R(1) \\ \vdots & & & \vdots \\ v_J^1(T) & v_J^2(T) & & v_J^R(T) \end{bmatrix} \tag{23}$$

$$V^R = U_s \Sigma S \tag{24}$$

$$\Sigma = diag(\lambda_1, \lambda_2, \dots, \lambda_m) \tag{25}$$

$$S = \begin{bmatrix} s_1^1(1) & s_1^2(1) & & s_1^m(1) \\ \vdots & & & \vdots \\ s_J^1(1) & s_J^2(1) & \dots & s_J^m(1) \\ \vdots & & & \vdots \\ s_J^1(T) & s_J^2(T) & & s_J^m(T) \end{bmatrix} \Rightarrow \tag{26}$$

$$S_m = \begin{bmatrix} s_1^m(1) & s_2^m(1) & \dots & s_J^m(1) \\ s_1^m(2) & s_2^m(2) & \dots & s_J^m(2) \\ & & \vdots & \\ s_1^m(T) & s_2^m(T) & \dots & s_J^m(T) \end{bmatrix} \tag{27}$$

The angular velocities were computed from joint angles measured with a CyberGlove from CyberGlove Systems (San Jose CA, USA) by numerical differentiation and applying a 5-sample smoothing filter. The rapid task length, and therefore synergy length, was set to the average sample length of the windowed rapid tasks across subject ($T = 60$ samples). We examined the variance accounted for by the first m synergies, σ_λ^2, using the sum-squared variance:

$$\sigma_\lambda^2 = \frac{\lambda_1^2 + \lambda_2^2 + \ldots + \lambda_m^2}{\lambda_1^2 + \lambda_2^2 + \ldots + \lambda_{50}^2} \tag{28}$$

The synergy state space and control matrices A, B, C, C_{KA}, and C_{KB} were formed according to (6)-(10), (21)-(22). It is worth noting that in this form, $S = B_s$ from equation (8). The synergies S were then used to reconstruct the natural-paced and ASL tasks using l_1-norm minimization. The problem is formulated as

$$\bar{v}_{row} \approx \bar{c} B_{syn} \tag{29}$$

where $\bar{v}_{row}$ is the vector of natural task velocities (V^N) formatted identically to the rows of V^R for a total task time of T_t. The matrix B_{syn} is the synergy bank of S and holds no direct relation to B of the state space model. The rows of B_{syn} contain every temporal offset of the first m synergies and so represent recruitment of a particular synergy at a particular time. The vector $\bar{c}$, therefore, contains the weights for each row of B_{syn} and so contains the synergy recruitments for each synergy at each point in time. The elements of $\bar{c}$ were optimally computed using the l_1-norm minimization algorithm:

$$Minimize \, \|\bar{c}\|_1 + \frac{1}{\lambda} \left\| \bar{c} B_{syn} - \bar{v}_{row} \right\|_2^2 \tag{30}$$

This algorithm minimizes the error between the measured data and the approximation while minimizing the magnitude of the recruitment weights with a regularization parameter λ. This reconstruction was repeated for every task, every subject, and using every set of synergies from $m = 1$ to $m = 10$.

The $\bar{c}$ vector contains the timeseries recruitments for each synergy, so we reshape it into a matrix U which contains the synergy recruitment commands for each time instant in its columns:

$$\bar{c} = \begin{bmatrix} c_1(0) & \dots & c_1(T_t) & \dots & c_m(T_t) \end{bmatrix} \Rightarrow \tag{31}$$

$$U = \begin{bmatrix} c_1(0) & c_1(1) & \dots & c_1(T_t) \\ c_2(0) & c_2(1) & \dots & c_2(T_t) \\ & & \vdots & \\ c_m(0) & c_m(1) & \dots & c_m(T_t) \end{bmatrix} \tag{32}$$

$$U = \begin{bmatrix} \bar{u}(0) & \bar{u}(1) & \dots & \bar{u}(T_t) \end{bmatrix} \tag{33}$$

Finally, the initial posture of the virtual hand $\bar{x}_0$ for each task was computed as the mean of the first 20 samples of the recorded hand angles.

The synergy recruitment timeseries was padded with zeros such that the recruitments began at $t = 1$ s. This allowed the model to stabilize at the initial hand posture before the task started. Each simulated grasp was run for a 4 second total duration. The dynamics model and control system were implemented in MATLAB/Simulink with a discrete sample rate of $F_s = 86$ Hz to match the experiment data.

III. RESULTS

A. RAPID GRASP KINEMATICS AND PRINCIPAL COMPONENT ANALYSIS

Several kinematic factors were computed from the rapid grasping data. The mean of the maximum absolute angular velocity across tasks, joints, and subjects was 3.81±2.67 rad/s with an absolute maximum angular velocity of 12.66 rad/s. The measured joint angles ranged from −1.17 to 2.24 rad or −67.0 to 128.6 degrees. This discrepancy in range of motion may be due to glove calibration biases, since the average range of motion across tasks, subjects, and joints is as expected at 0.785±0.529 rad or 45.0±30.4 degrees.

Principal component analysis yielded synergies with sum-squared variances shown in Fig. 3. The first four synergies accounted for 80.7±7.79, 8.15±3.41, 2.85±1.87, and 1.87±0.6% variance. 80% cumulative variance was achieved by the first synergy, and 95% cumulative variance was achieved by the fifth synergy.

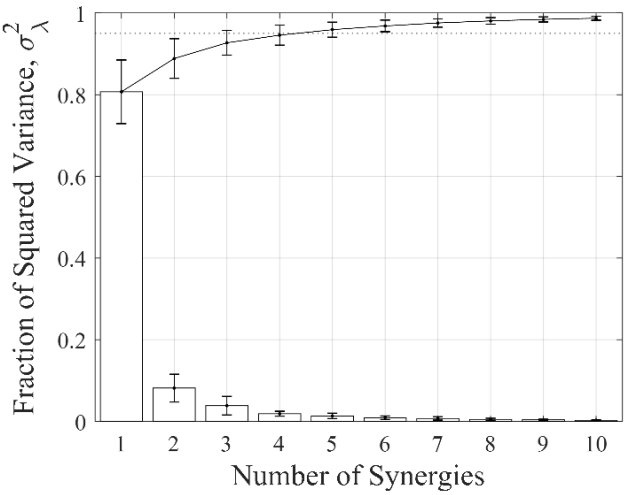

FIGURE 3. Sum-squared variance for each of the first 10 synergies averaged across subjects, shown as bars. The cumulative sum of the first *m* synergies is shown as the solid line, with the 95% threshold overlaid with a dotted line.

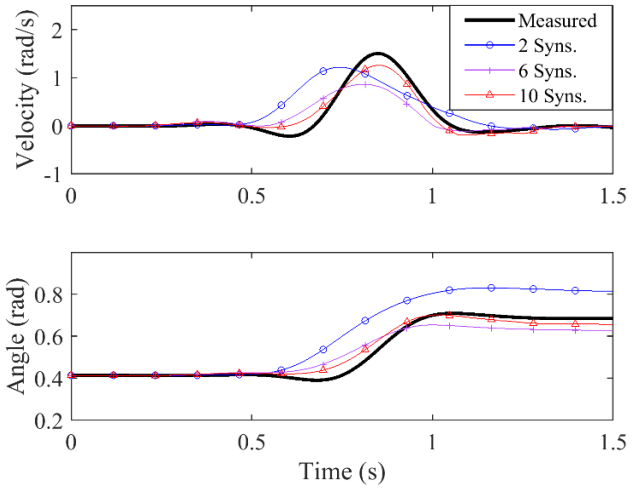

FIGURE 4. Examples of velocity reconstruction (top) and corresponding angular profiles (bottom) using 2, 6, and 10 synergies. Data is from subject 1, task 45, middle PIP joint.

B. NATURAL GRASP/ASL POSTURE KINEMATICS AND RECONSTRUCTION

Similar kinematic parameters were examined for the natural-paced and ASL tasks. The average absolute angular velocity across joints, tasks, and subjects was 2.49±2.14 rad/s, with a maximum velocity across all tasks, joints, and subjects of 13.51 rad/s. The measured joint angles during all tasks ranged from −1.095 to 2.642 rad or −62.7 to 151.4 degrees, with a mean range of motion across joints, tasks, and subjects of 0.767±0.567 rad or 43.9±32.49 degrees. The angle bounds of the virtual hand model were set to 90 degrees of extension and 180 degrees of flexion to avoid artificially cropping the simulated response. Each task lasted for $T_{task} = 199$ recorded samples, or 2.33s of data.

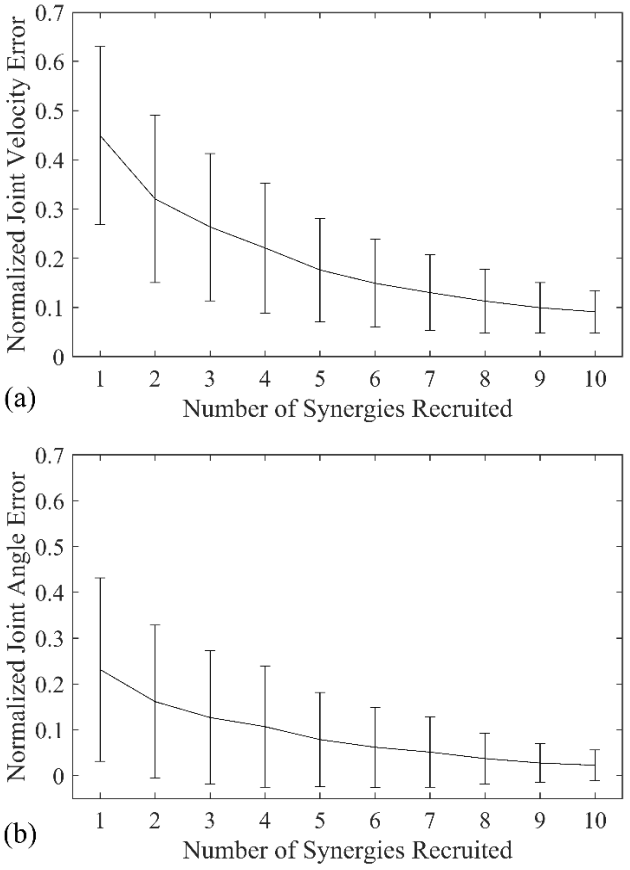

FIGURE 5. Reconstruction error when using the first m synergies. The velocity (a) and angle (b) errors are shown, which are computed as normalized sums over time and joints of the squared error, averaged across subjects and tasks.

An example of task reconstruction is shown in Fig. 4. The velocity profile (top) is reconstructed using sequentially many synergies, with synergies 2, 6, and 10 shown. The angle profile for each synergy is integrated numerically, with the initial posture set to the average of the first 20 samples of the recorded data. The first two synergies can replicate the shape of the velocity and/or angle profile, however higher-order synergies are needed to fine-tune the approximation and approach the correct hand trajectory. Adding more synergies also decreases error in the final hand posture. However, adding more synergies leads to diminishing returns, as there is less improvement from 6 to 10 synergies as in 2 to 6. Fig. 5(a) shows the velocity reconstruction error averaged across subjects and tasks for each number of synergies while Fig. 5(b) shows the angular reconstruction error. The velocity reconstruction error drops from 42.2±18.5% for one synergy to 9.79±8.53% for six synergies and 3.64±3.24% for ten. The angle reconstruction error follows a similar trend with 23.1±20.0% for the first synergy, 6.05±8.76% for the first six synergies, and 2.14±3.33% for the first ten.

C. CONTROL SIMULATION

The standard torque control law (6) was autotuned finger-by-finger as five individual two input, two output MIMO systems

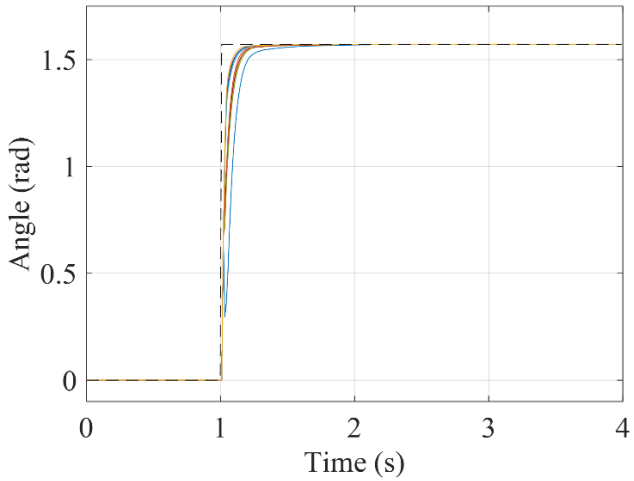

FIGURE 6. Step response of the tuned torque controller for all joints. The 95% rise time averaged across all joints is 0.131s.

with a time constant of 0.116s, or ten times the time step of the simulated data. The 1.571 rad (90 degree) simultaneous step response of all joints is shown in Fig. 6. The average rise time, calculated as the time at which a joint reached 95% of the step response, is 0.131s. An example of one simulated task from subject 6, task 74, with 10 synergies is shown in Fig. 7. In this plot, the solid black line represents the measured trajectory, the dotted black line represents the virtual synergy trajectory computed from the synergy weight inputs, and the blue/red lines are the simulated angles and velocities for the corresponding DoF. There is close accuracy in the angular profiles between the measured and simulated data with the exception of the thumb MCP joint. Two accuracy comparisons were made to quantify the system performance: the accuracy of the simulated states relative to the synergy-generated setpoint trajectories, and the accuracy of the states relative to the measured data.

The accuracy of the simulated states to the virtual synergy trajectories gave a measure of the tuned controller's ability to actuate according to the synergy weights given as inputs. The overall error of the system averaged across tasks, joints, subjects, and synergies was 0.15±0.0073% for angles and 8.13±3.65% for velocities. The error compared over numbers of recruited synergies showed that the lower-order synergies were more accurately controlled than the higher-order synergies (Fig. 8). Comparing results with two one-way ANOVAs with $\alpha = 0.05$ found significant differences among angular error ($p \ll 0.001$) and velocity error ($p = 0.004$). A Tukey-Kramer post-hoc test was performed for angle and velocity error. For the velocity error, significant differences were found between synergy 1 (7.56%) and synergies 4-10. For the angle error, significant differences were found between

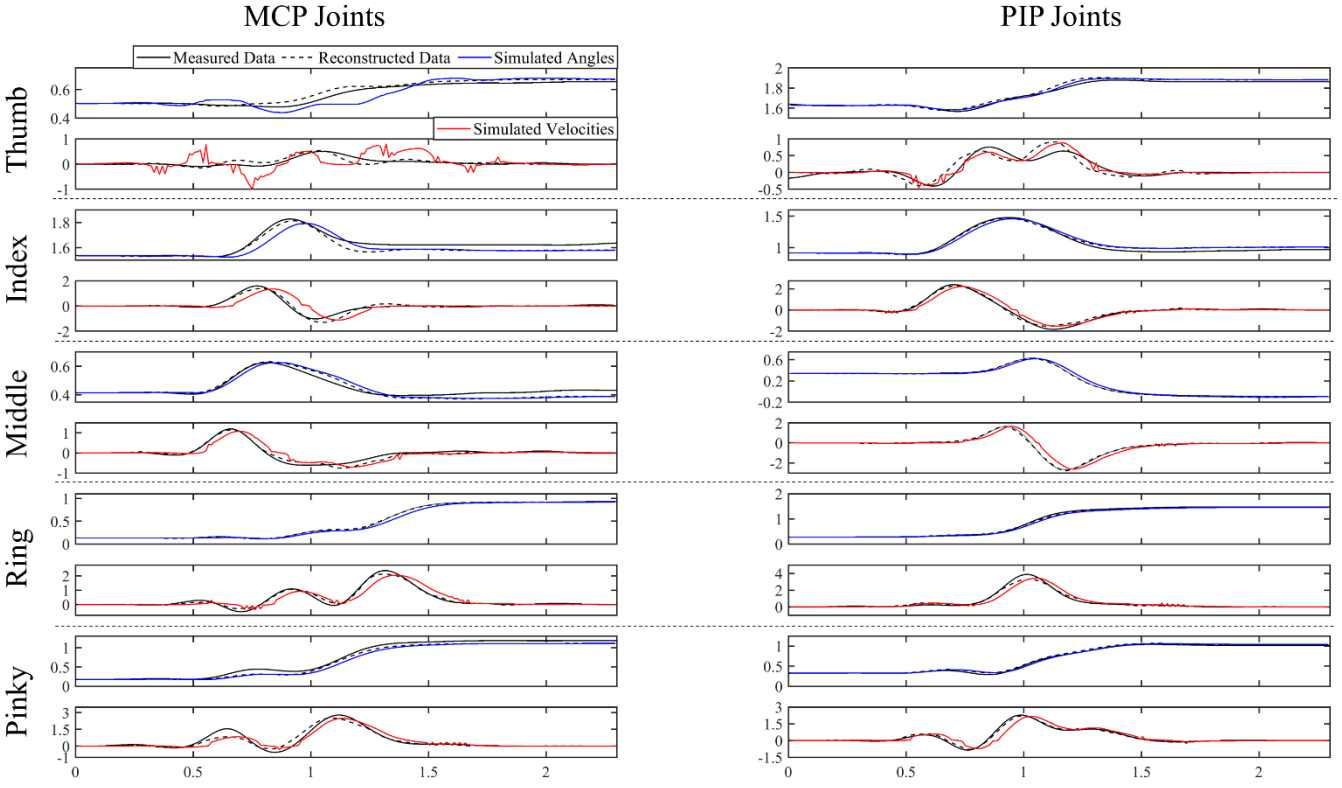

FIGURE 7. Example data from simulation of subject 6, task 74 using 10 synergies. The left and right columns are the MCP and PIP joints for each finger, respectively. Each finger is labeled on the left, with dotted lines delineating the different DoF. The upper and lower plots for each DoF show angles and velocities, respectively. The solid black line is the measured data, the dotted black line is the synergy trajectory generated by the optimally computed synergy weights, and the blue and red lines are the simulated angles and velocities of the virtual hand, respectively. Time is along the x axis in seconds.

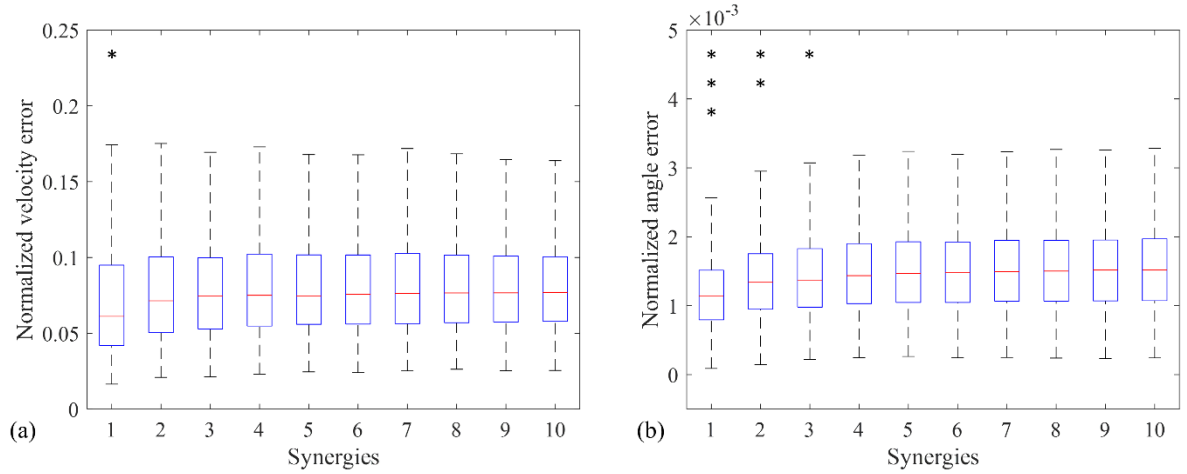

FIGURE 8. Simulation error compared to synergy trajectories for different numbers of synergies. (a) Velocity error, where synergy 1 was significantly different from synergies 4-10 ($p = 0.004$). Results found using one-way ANOVA with $\alpha = 0.05$. (b) Angle error, where synergy 1 was significantly lower than 2-10, synergy 2 was significantly different from synergy 1 and 4-10, and synergy 3 was significantly different from synergy 1 and 7-10 ($p \ll 0.001$).

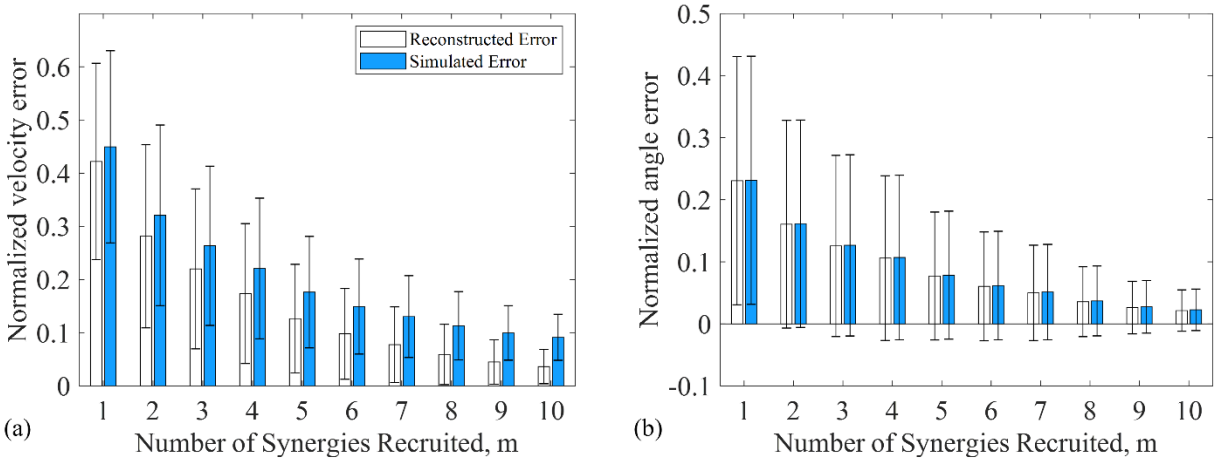

FIGURE 9. Normalized error between measured data and reconstructed (white) and simulated (blue) data. The reconstructed error is identical to the data shown in FIGURE 5. (a) Normalized velocity error. The simulated states have an increased error relative to the reconstructed states which were used as setpoints. (b) Normalized angle error, with little increased reconstruction error relative to the synergy trajectory. This mirrors the larger velocity error relative to the angle error when comparing the simulation to the synergy trajectories.

synergy 1 (0.12%) and synergies 2-10, synergy 2 (0.14%) was significantly different from synergies 1 and 4-10, and synergy 3 (0.15%) was significantly different from synergy 1 and synergies 7-10. Statistically meaningful increases in error occurred due to increasing the number of synergies, however this effect appears to be small relative to the practical applications and is only present in the lower synergies. The angular error of the thumb MCP joint was computed as 5.6±27.6% averaged across synergies, tasks, and subjects compared to 0.22±0.47% for the remaining fingers. This discrepancy is likely due to the higher mass of the thumb compared to the other fingers, and would likely be solved by using a higher operational frequency for the controller.

The simulated states were then compared to the measured data from the original experiment. Fig. 9 is a bar plot which shows the reconstruction errors, identical to Fig. 5, next to the simulation errors, both of which are computed relative to the measured data. The discrepancy between the two bars is due to the compounded error of the synergy reconstruction and the controller error. The difference in velocities was statistically significant for all synergies ($p < 0.001$ for synergy 1, $p \ll 0.001$ for all others) using t-tests with a corrected $\alpha = 0.005$ for multiple comparisons. The difference in angle errors was not statistically significant by the same method ($p \gg 0.005$). Although the controller did not ideally replicate the velocity profile, it did not result in a statistically meaningful increase in angular error.

An example task simulation is shown in Fig. 10, including the hand poses produced by the control law. The raw angles, reconstructed angles, and simulated angle are shown on the

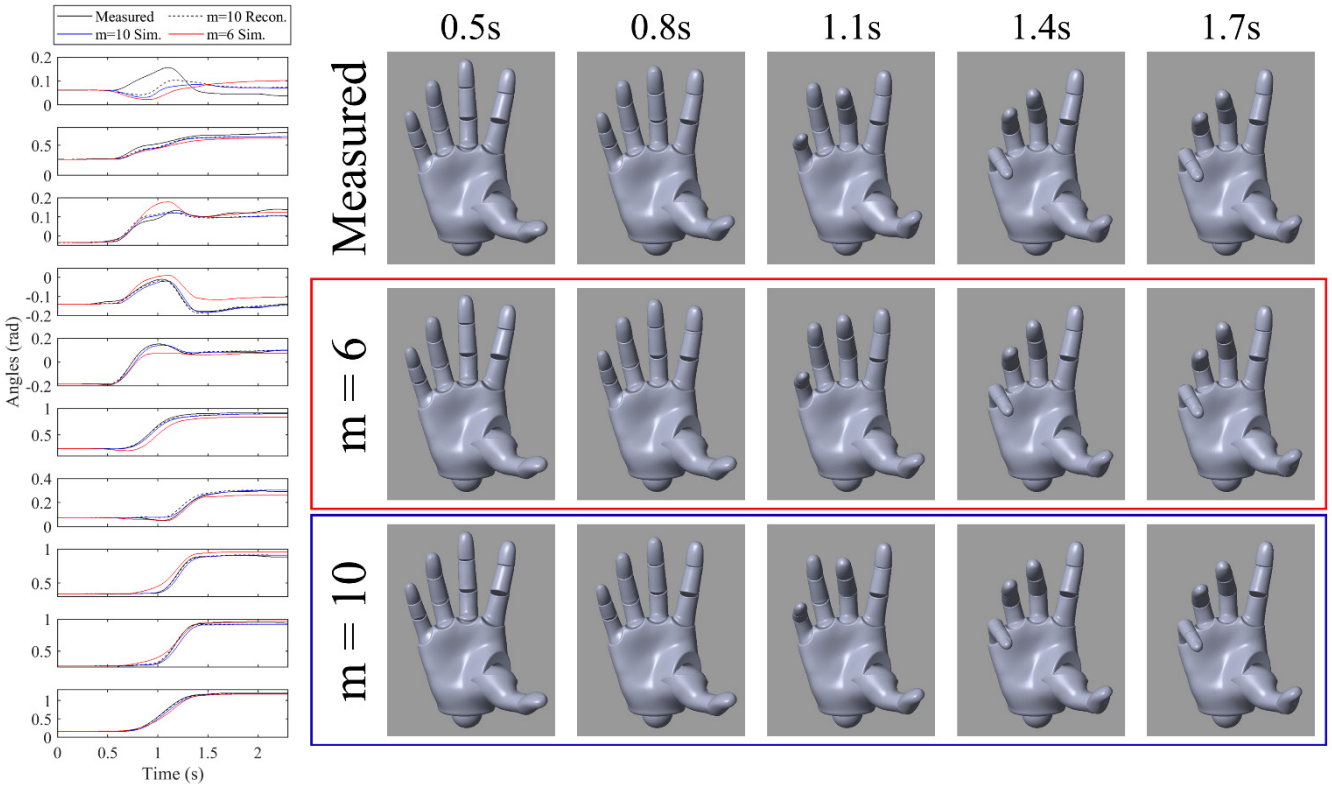

FIGURE 10. Example simulation of subject 5, task 14, repetition 2. The angles for the task are shown at left, in the order of thumb MCP, thumb PIP, index MCP, index PIP, ...in radians. The original recorded data is shown in solid black, the reconstructed angular profile for $m = 10$ synergies is shown in dotted black, the simulated angles using $m = 6$ synergies are shown in solid red, and the simulated angles using $m = 10$ synergies is shown in solid blue. At right, images of the hand are shown for the measured profile, the $m = 6$ simulation, and the $m = 10$ simulation from $t = 0.5s$ to $t = 1.7s$. Using a full-synergy controller yields the best results, however a dimensionally reduced control law yields comparable results throughout the grasp.

left, with images of the simulated hand from $t = 0.5$ to 1.7s shown. Two synergy conditions are shown in this plot to demonstrate the visual similarity between the measured data, the dimensionally reduced simulation, and the full-synergy simulation. The $m = 6$ synergy condition may be a useful example as it reduces hand grasping complexity to the 6-DoF case, which is commonly handled with traditional control methods. The average angle error for $m = 6$ is 6.18±8.75%, and for $m = 10$ is 2.29±3.35%. Fewer synergies may be used at the discretion of the control designer, with the 10% accuracy level achieved by $m = 4$ with 10.7±13.26% ($p = 0.062$, one-tailed t test).

The torques applied to the joints of the virtual hand can be useful for designing assistive devices. The absolute maximum instantaneous torque applied across all joints, tasks, synergies, and subjects was 6.61 Nm with an average of 2.17±1.15 Nm. Converting these torques to actuator torques or forces will require a detailed geometric model of the robotic system, which is reserved for future work.

IV. DISCUSSION

This paper presented a novel method to recruit synergies from a time series of synergy recruitment weights. The state space formulation shown here has several benefits which can facilitate its application to robotic control problems. First, this method generalizes synergy recruitment from the postural synergy case, used in many papers to-date, to the spatiotemporal case, shown here for the first time. Using synergies of length $T = 1$ yields the postural case, however the state space model can be initialized to any number of synergies defined across any number of joints for any number of sample lengths. Second, the formulation lends itself to discrete real-time applications in a compact form using basic matrix operations. Third, the expression as a standard state space model is readily substituted into control laws, and the properties of the system such as controllability, reachability, and observability are trivially computed. Furthermore, the state space model has an equivalent transfer function form which may lend itself to additional types of analysis than what is currently possible. The operational workspace in synergy coordinates is also readily computed for a given subject's synergies, allowing bounds to be set in the synergy domain which prevent the system from violating range of motion constraints. Finally, the state space model allows new mathematical optimization methods to be used to compute synergy weights for reconstruction of natural grasping data. Whereas l_1-norm minimization expresses synergy recruitment as a linear vector optimization problem, the state space model can be treated as a dynamic system to be controlled such that the error from a grasping task is minimized.

The proposed synergy recruiter is integrated into a torque controller with spring and damping matrices. Each finger was tuned as a 2-DoF MIMO system and combined into a 10-DoF controller. The controller was tuned as accurately as the sample rate allowed before unstable responses appeared. The resulting controller accuracy was high for the recruited joint angles, and within reasonable bounds for the recruited velocity trajectory. The thumb MCP and PIP joints appear to have higher error than the remaining joints, perhaps due to its higher mass compared to the other links of the hand. Better results may be obtained by increasing the sample rate of the simulation. In this work, we fixed the sample rate to match the prior grasping data measured at 86Hz. However, a real-time system aimed at grasp assistance can be operated at higher sample rates which can lead to improved controller performance due to tighter tuning. Synergies can be captured at standard sample rates for data gloves or optical hand tracking, then be interpolated to match the sample rate of the controller. The matrix sizes in the state space model will increase with higher sample-length synergies, which must be considered when determining the achievable controller cycle time on a hardware system. Higher accuracies may also be possible by integrating the synergy recruiter into alternative control laws beyond the torque controller shown here. Sliding mode control, H∞ control, or an LQR controller may be implemented for systems with varying requirements for robustness, response time, and processor power. It is important to consider the controllability of the synergy system when implementing these methods. A synergy-based system will not be fully linearly controllable for $m < J$, however practical results may be achievable by restricting methods to a controllable subset of the total state space.

The goal of this paper was to demonstrate a controller based on spatiotemporal synergies in simulation. Our results showed similar characteristics to postural and spatiotemporal synergies found elsewhere in the literature. Task reconstruction yielded similar error levels to those found in other studies [14], [16] while the variances accounted for by our synergies are in line with that found in other literature [22]. Furthermore, the extracted spatiotemporal synergies showed patterns of functional grouping which are present in related works in upper limb reaching and grasping. We found low-order synergies to encode gross hand movements such as the whole-hand grasp and a three-finger grasp, while higher order synergies encoded finer motions. The next steps involve deploying a spatiotemporal synergy-based controller to real-time hardware systems for assistance and rehabilitation. There are several challenges which must be overcome to accomplish this, especially if the hardware system is a soft wearable hand exoskeleton. The controller we propose here is based on several assumptions. First, we assumed a known dynamics model of a healthy hand with no model uncertainty or spring/damper effects from tissue properties. Second, we assumed we can perfectly apply torques to each joint independently and instantaneously. Third, we assumed perfect sensor feedback for position and velocity from every joint. These assumptions will generally not hold in practice, so several additional methods will need to be used to create a functional system.

A soft hand exoskeleton has several sources of model uncertainty which will need to be considered. The unique kinematic and dynamic properties of the user's hand will affect the response of the exoskeleton. This includes finger link lengths, ranges of motion, tissue compliance, and hand spasticity in the case of a stroke-affected individual. The compliance of the soft exoskeleton will also cause the robot to deform during use, causing the geometric properties of the system to change. We can approach this problem by using an idealized model of the hand with tunable properties that are estimated from calibration data. We can establish bounds on our model uncertainty, and therefore the robustness of our controller, using this information.

There is uncertainty in the actuation of the hand in addition to the uncertainty in the dynamic response of the system. Variations in actuators, response times, friction, and co-contractions due to the device's construction and the user's anatomy will all impact the system's ability to control each joint. Most soft exoskeleton devices use Bowden cables or fluid-based actuators which may apply force to multiple joints at once. An actuator Jacobian may be calibrated to model the co-contraction of individual joints as a function of force from one actuation. The Jacobian matrix can then be inverted to compute actuator torques based on the desired joint torques. The low-level force controllers responsible for applying the desired force will also have to operate faster than the high-level controller to minimize the response time of the system, and so maintain actuation accuracy. These will need to be tuned to overcome variations in friction and actuators.

Finally, measuring joint angles and velocities of the hand is difficult to do reliably. The sensors that can be implemented in soft systems have variation in responses, reliability issues, and in some cases excessive noise which makes it difficult to get good measurements of the kinematic states. Because of this, special design considerations will need to be made in the mechanical system as well as the signal processing to maximize sensor performance and minimize external effects. Estimators may need to be designed which can produce accurate joint angles and velocities despite noisy and/or missing sensor data.

In this paper we assume we have the synergy recruitment weights necessary to replicate natural grasping. This allows us to test our controller with a controlled dataset, however this assumption does not hold in practical scenarios. A full BCI system which uses this controller in real time will need a method of extracting synergy weights from user inputs. These inputs can be in the form of basic inputs such as button presses, joystick controls, keyboard/touch screen controls, tongue controls or breath switches. Motion tracking methods may also be used to extract synergy weights such as ocular tracking or arm tracking during reaching. Noninvasive biosignals may be used such as EMG or EEG, as well as

invasive techniques such as implanted spinal or peripheral nerve electrodes or ECoG.

V. CONCLUSION

This paper has presented a novel state-space expression for synergy recruitment. This method is generalizable to postural as well as spatiotemporal synergy recruitment and is expressed in a form which can readily be used in standard control laws and controls analysis. A dynamics model of a 50th percentile male hand was used to simulate a torque control law based on spatiotemporal synergy recruitment. This model was used to replicate natural grasps and ASL hand motions using only optimally computed synergy weights. Reconstruction and simulation accuracy were characterized, yielding data useful to determine how many synergies should be used to control a robotic system. The next steps are discussed to realize this controller with a robotic device such as a soft hand exoskeleton or prosthetic. Major challenges include model uncertainty in the hand and sensor reliability.

ACKNOWLEDGEMENT

The authors would like to thank the Department of Biomedical Engineering for their ongoing support of our research.

REFERENCES

[1] K. Ziegler-Graham, E. J. MacKenzie, P. L. Ephraim, T. G. Travison, and R. Brookmeyer, "Estimating the prevalence of limb loss in the United States: 2005 to 2050," *Arch. Phys. Med. Rehabil.*, vol. 89, no. 3, pp. 422–429, 2008.

[2] A. Esquenazi, "Amputation rehabilitation and prosthetic restoration. From surgery to community reintegration," *Disab. Rehabil.*, vol. 26, nos. 14–15, pp. 831–836, 2004.

[3] V. Y. Ma, L. Chan, and K. J. Carruthers, "Incidence, prevalence, costs, and impact on disability of common conditions requiring rehabilitation in the United States: Stroke, spinal cord injury, traumatic brain injury, multiple sclerosis, osteoarthritis, rheumatoid arthritis, limb loss, and back pain," *Arch. Phys. Med. Rehabil.*, vol. 95, no. 5, pp. 986–995, 2014.

[4] B. H. Dobkin, "Rehabilitation after Stroke," *New England J. Med.*, vol. 352, no. 16, pp. 1677–1684, Apr. 2005.

[5] A.-C. Jönsson, I. Lindgren, B. Hallström, B. Norrving, and A. Lindgren, "Determinants of quality of life in stroke survivors and their informal caregivers," *Stroke*, vol. 36, no. 4, pp. 803–808, 2005.

[6] E. A. Biddiss and T. T. Chau, "Upper limb prosthesis use and abandonment: A survey of the last 25 years," *Prosthetics Orthotics Int.*, vol. 31, no. 3, pp. 236–257, 2007.

[7] M. C. Tresch and A. Jarc, "The case for and against muscle synergies," *Current Opinion Neurobiol.*, vol. 19, no. 6, pp. 601–607, 2009.

[8] P. Saltiel, K. Wyler-Duda, A. D'Avella, M. C. Tresch, and E. Bizzi, "Muscle synergies encoded within the spinal cord: Evidence from focal intraspinal NMDA iontophoresis in the frog," *J. Neurophysiol.*, vol. 85, pp. 605–619, Feb. 2001.

[9] T. Drew, J. Kalaska, and N. Krouchev, "Muscle synergies during locomotion in the cat: A model for motor cortex control," *J. Physiol.*, vol. 586, no. 5, pp. 1239–1245, 2008.

[10] N. Krouchev, J. F. Kalaska, and T. Drew, "Sequential activation of muscle synergies during locomotion in the intact cat as revealed by cluster analysis and direct decomposition," *J. Neurophysiol.*, vol. 96, no. 4, pp. 1991–2010, 2006.

[11] S. A. Overduin, A. d'Avella, J. M. Carmena, and E. Bizzi, "Microstimulation activates a handful of muscle synergies," *Neuron*, vol. 76, no. 6, pp. 1071–1077, 2012.

[12] M. T. Turvey, "Action and perception at the level of synergies," *Hum. Movement Sci.*, vol. 26, no. 4, pp. 657–697, Aug. 2007.

[13] V. Patel, M. Burns, Z.-H. Mao, N. E. Crone, and R. Vinjamuri, "Linear and nonlinear kinematic synergies in the grasping hand," *J. Bioeng. Biomed. Sci.*, vol. 5, no. 3, p. 1, 2015.

[14] R. Vinjamuri, D. J. Weber, Z.-H. Mao, J. L. Collinger, A. D. Degenhart, J. W. Kelly, M. L. Boninger, E. C. Tyler-Kabara, and W. Wang, "Toward synergy-based brain-machine interfaces," *IEEE Trans. Inf. Technol. Biomed.*, vol. 15, no. 5, pp. 726–736, Sep. 2011.

[15] V. Patel, M. Burns, and R. Vinjamuri, "Effect of visual and tactile feedback on kinematic synergies in the grasping hand," *Med. Biol. Eng. Comput.*, vol. 54, no. 8, pp. 1217–1227, 2016.

[16] M. K. Burns, V. Patel, I. Florescu, K. V. Pochiraju, and R. Vinjamuri, "Low-dimensional synergistic representation of bilateral reaching movements," *Frontiers Bioeng. Biotechnol.*, vol. 5, no. 2, pp. 1–15, Feb. 2017.

[17] M. Xiloyannis, L. Cappello, D. B. Khanh, S.-C. Yen, and L. Masia, "Modelling and design of a synergy-based actuator for a tendon-driven soft robotic glove," in *Proc. 6th IEEE Int. Conf. Biomed. Robot. Biomechatron. (BioRob)*, Jun. 2016, pp. 1213–1219.

[18] S. Li, X. Sheng, H. Liu, and X. Zhu, "Design of a myoelectric prosthetic hand implementing postural synergy mechanically," *Ind. Robot Int. J.*, vol. 41, no. 5, pp. 447–455, 2014.

[19] W. Chen, C. Xiong, and S. Yue, "Mechanical implementation of kinematic synergy for continual grasping generation of anthropomorphic hand," *IEEE/ASME Trans. Mechatronics*, vol. 20, no. 3, pp. 1249–1263, Jun. 2015.

[20] M. G. Catalano, G. Grioli, E. Farnioli, A. Serio, C. Piazza, and A. Bicchi, "Adaptive synergies for the design and control of the pisa/IIT SoftHand," *Int. J. Robot. Res.*, vol. 33, no. 5, pp. 768–782, Apr. 2014.

[21] K. Xu, Z. Liu, B. Zhao, H. Liu, and X. Zhu, "Composed continuum mechanism for compliant mechanical postural synergy: An anthropomorphic hand design example," *Mechanism Mach. Theory*, vol. 132, pp. 108–122, Feb. 2019.

[22] T. Wimböck, B. Jahn, and G. Hirzinger, "Synergy level impedance control for multifingered hands," in *Proc. IEEE/RSJ Int. Conf. Intell. Robots Syst.*, Sep. 2011, pp. 973–979.

[23] P. K. Artemiadis and K. J. Kyriakopoulos, "EMG-based control of a robot arm using low-dimensional embeddings," *IEEE Trans. Robot.*, vol. 26, no. 2, pp. 393–398, Apr. 2010.

[24] J. Rosell, R. Suárez, C. Rosales, and A. Pérez, "Autonomous motion planning of a hand-arm robotic system based on captured human-like hand postures," *Auton. Robots*, vol. 31, no. 1, pp. 87–102, 2011.

[25] F. Ficuciello, D. Zaccara, and B. Siciliano, "Synergy-based policy improvement with path integrals for anthropomorphic hands," in *Proc. IEEE/RSJ Int. Conf. Intell. Robots Syst. (IROS)*, Oct. 2016, pp. 1940–1945.

[26] L. Hua, X. Sheng, W. Lv, and X. Zhu, "Automatic grasp planning algorithm for synergistic underactuated hands," in *Proc. Int. Conf. Intell. Robot. Appl.*, 2016, pp. 431–442.

[27] G. Borghesan, E. Aertbeliën, and J. De Schutter, "Constraint-and synergy-based specification of manipulation tasks," in *Proc. IEEE Int. Conf. Robot. Automat. (ICRA)*, May/Jun. 2014, pp. 397–402.

[28] C. E. Clauser, J. T. McConville, and J. W. Young, "Weight, volume, and center of mass of segments of the human body," Air Force Syst. Command, Wright-Patterson Air Force Base, OH, USA, Tech. Rep. AMRL TR 69-70, 1969.

MARTIN K. BURNS received the B.S. degree in biomedical engineering and the M.E. degree in engineering management from the Stevens Institute of Technology, Hoboken, NJ, USA, in 2015.

From 2011 to 2012, he was with the Merck & Co, Prototyping High Throughput Laboratory Robotics, and in 2013, worked for Stryker designing implants in advanced concept development. He is currently a Research Assistant and a Ph.D. Candidate with the Biomedical Engineering Department, Stevens Institute of Technology. His work was supported by the New Jersey Health Foundation, the National Science Foundation, and the Innovation and Entrepreneurship Doctoral Fellowship. His research interests include robotics and control systems for assistive and rehabilitative robotics and brain–machine interfaces.

DINGYI PEI (S'18) received the B.S. degree in biomedical engineering from Tianjin University, China, in 2016, and the M.E. degree in biomedical engineering from the Stevens Institute of Technology, in 2018, where she is currently pursuing the Ph.D. degree in biomedical engineering. Her bachelor's and graduate research projects consisted of prosthetic control methods, brain–computer interfaces, biosignal detection circuit designs, biosignal, and medical image processing. She received the Steven's Provost Doctoral Fellowship for current research. She also received the third prize in the International Contest of Applications in Nano-Micro Technologies, in 2014.

RAMANA VINJAMURI (M'08–SM'11) received the B.S. degree from Kakatiya University, India, in 2002, the M.S. degree from Villanova University, Villanova, PA, USA, in 2004, and the Ph.D. degree from the University of Pittsburgh, Pittsburgh, PA, USA, in 2008, all in electrical engineering. He was a Research Associate with the Department of Physical Medicine and Rehabilitation, University of Pittsburgh, from 2008 to 2012. He was a Research Assistant Professor with the Department of Biomedical Engineering, Johns Hopkins University, from 2012 to 2013. He then joined the Department of Biomedical Engineering, Stevens Institute of Technology, as an Assistant Professor, in 2013. He is currently a Harvey N. Davis Distinguished Assistant Professor with the Department of Biomedical Engineering, Stevens Institute of Technology. His research was supported by the National Science Foundation, the New Jersey Health Foundation, and the Stevens Institute of Technology. He received the NSF CAREER Award, in 2019.